Three-dimensional nonlinear photonic crystal in ferroelectric barium calcium titanate

Tianxiang **Xu**[1,2], Krzysztof **Switkowski**[3,4], Xin **Chen**[1], Shan **Liu**[1], Kaloian **Koynov** [5], Haohai **Yu**[2], Huaijin **Zhang**[2], Jiyang **Wang**[2], Yan **Sheng**[1]* and Wieslaw **Krolikowski**[1,4]*

The performance of many optical devices based on frequency conversion critically depends on spatial modulation of the nonlinear optical response of materials. This modulation ensures efficient energy exchange between optical waves at different frequencies via quasi-phase matching[1]. In general, quasi-phase matching structures, also known as nonlinear photonic crystals[2–4], offer a variety of novel properties and functionalities that cannot be obtained in uniform nonlinear crystals[5–9]. So far, nonlinear photonic crystals have been restricted to one- or two-dimensional geometries due to a lack of fabrication technologies capable of 3D nonlinearity engineering. Here, we provide an experimental example of a 3D nonlinear photonic crystal, fabricated in ferroelectric barium calcium titanate, by applying an ultrafast light domain inversion approach. The resulting full flexibility of 3D nonlinearity modulation enables phase matching of nonlinear processes along an arbitrary direction, thereby removing constraints imposed by low-dimensional structures.

Second-order nonlinear optical effects, for example in second harmonic (SH), sum and difference frequency generation, are of great importance in applications such as laser wavelength extension, ultrafast signal processing, quantum light sources and terahertz technology, among others. An essential condition in these processes is synchronization of the phases of the interacting waves. This can be achieved using quasi-phase matching (QPM)[1], which involves spatial modulation of the second-order nonlinear coefficient $\chi^{(2)}$ of nonlinear crystal.

The QPM interaction was first accomplished for a single nonlinear process in one-dimensional (1D) periodic $\chi^{(2)}$ gratings (also called optical superlattices[10]). Motivated by the need for a broad spectral operating range as well as multiple spatial directions, QPM was generalized to 2D $\chi^{(2)}$ modulation in what are known as nonlinear photonic crystals (NPCs)[2–4]. Although 2D NPCs offer more flexibility in applications, they suffer from fundamental problems such as low conversion efficiency in spatial beam processing and are feasible only for compensation of phase mismatches in a single plane (Fig. 1a).

The full potential of the QPM technique can only be utilized with 3D spatial nonlinearity modulation[11,12]. This 3D modulation offers exclusive access to reciprocal lattice vectors in the third dimension and therefore enables phase matching of nonlinear processes along an arbitrary direction (Fig. 1b). In this way, 3D NPCs constitute ideal systems for the realization of a variety of second-order nonlinear interactions and effects. From a practical point of view, 3D NPCs enable entire novel classes of photonic devices, including true $\chi^{(2)}$ volume holography[13], 3D nonlinear photonic integrated circuits and 3D domain-wall-based photovoltaic devices and non-volatile memories[14].

The realization of 3D $\chi^{(2)}$ modulation is beyond the reach of traditional fabrication techniques. For instance, the most popular approach of electric field poling of ferroelectrics cannot modulate $\chi^{(2)}$ along the depth of the medium. As the external poling field must be applied via patterned electrodes, the domain switching process in this method always begins with nucleation (the inception of new domains) on the surface[15].

Alternative techniques that allow one to overcome some drawbacks of electric poling have been proposed. One possibility is to use all-optical poling, which uses intense UV laser radiation, the absorption of which induces a high temperature gradient and subsequent domain reversal via a thermoelectric field[16–18]. However, because of strong UV absorption, this technique works only in a thin, subsurface layer of the medium, and so UV poling is not suitable for the fabrication of 3D NPCs. Another method is to employ metamaterials-based NPCs in which the inverted orientation of split-ring resonators leads to inversion of the sign of the effective quadratic nonlinearity[19,20].

We have recently achieved a breakthrough in all-optical poling of ferroelectric crystals by utilizing the nonlinear absorption of focused infrared femtosecond laser pulses[21–23], which allows the realization of domain reversal deep below the crystal's surface and for non-standard crystallographic orientation. In this Letter we demonstrate that this approach opens up the possibility of achieving fully 3D NPCs.

Here, direct femtosecond laser writing of 3D ferroelectric domain patterns was accomplished in an X-cut tetragonal perovskite ferroelectric $Ba_{0.77}Ca_{0.23}TiO_3$ (BCT) crystal. The use of short infrared pulses allowed us to focus the light deep inside the transparent BCT and consequently to form various 3D ferroelectric domain structures (see Fig. 1c for an example, and also the Methods). The pulse duration, repetition rate and pulse energy of the laser beam were 180 fs, 76 MHz and ~6 nJ, respectively. More microscopic images of the laser-induced ferroelectric domain patterns are presented in Supplementary Figs. 3 and 5.

The focusing of femtosecond laser pulses inside the X-cut BCT crystal led to the formation of theta (θ)-shaped domain structures (Fig. 2a). Because the crystal contains initially randomly oriented nanosized 180° domains (Supplementary Fig. 1), the θ shape originates from the realignment and merger of these small random

[1]Laser Physics Center, Research School of Physics and Engineering, Australian National University, Canberra, Australian Capital Territory, Australia. [2]State Key Laboratory of Crystal Materials and Institute of Crystal Materials, Shandong University, Jinan, China. [3]Faculty of Physics, Warsaw University of Technology, Warsaw, Poland. [4]Science Program, Texas A&M University at Qatar, Doha, Qatar. [5]Max-Planck Institute for Polymer Research, Mainz, Germany. *e-mail: yan.sheng@anu.edu.au; Wieslaw.Krolikowski@anu.edu.au
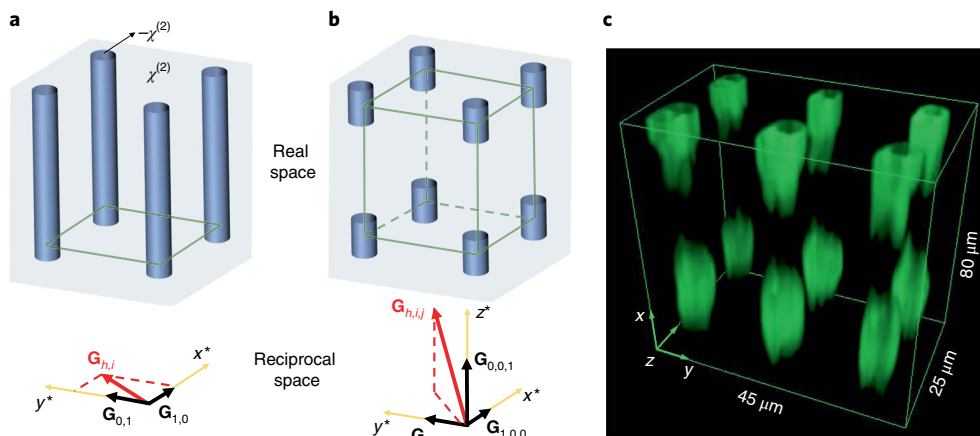
Fig. 1 | NPCs and their corresponding reciprocal lattice vectors. a, Illustration of a 2D NPC, whose reciprocal lattice vectors ($\mathbf{G}_{h,i}$) are confined to the plane perpendicular to the spatial modulation of the second-order nonlinear coefficient $\chi^{(2)}$. **b**, A new degree of freedom is achieved by modulating $\chi^{(2)}$ in three dimensions. The resulting reciprocal lattice vectors $\mathbf{G}_{h,i,j}$ are now located in 3D space, making it possible to compensate for phase mismatch of quadratic nonlinear processes along an arbitrary direction. **c**, Čerenkov SH microscopic image of the 3D ferroelectric domain pattern, fabricated in $Ba_{0.77}Ca_{0.23}TiO_3$ crystal using femtosecond laser pulses (see Methods). The domain modulation periods are $\Lambda_x = 64.0$ and $\Lambda_y = \Lambda_z = 15.0\,\mu m$. The total size of the laser-produced 3D domain structure is $256\,\mu m\,(x) \times 90\,\mu m\,(y) \times 120\,\mu m\,(z)$.
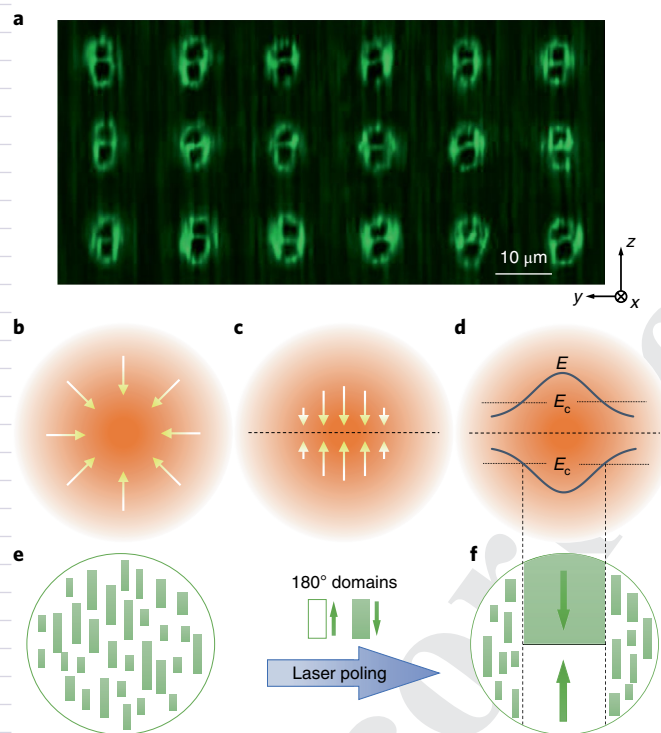

Fig. 2 | Ferroelectric domain inversion with ultrafast light in the BCT crystal. a, The θ-like domain structure created by femtosecond laser pulses, visualized by Čerenkov SH microscopy. The background (weak random patterns surrounding the θ domains) originates from random inherent submicrometre-period domains in the BCT crystal (Supplementary Fig. 1). **b–f**, Mechanism of domain reversal with focused infrared femtosecond pulses: nonlinear absorption of tightly focused pulses significantly increases the temperature, and its gradient in the focal area in the crystal (indicated by arrows) acts as a source of a thermoelectric field (**b**); a change in the sign of the temperature gradient along the direction of spontaneous polarization (*z*) (**c**) induces a bipolar electric field (**d**), which exceeds the coercive field (E_c) and inverts microdomains to form two larger antiparallel domains, as shown in **e** (before poling) and **f** (after poling).

domains into two large domains with opposite polar orientations. The central horizontal line of the θ-like structure is always perpendicular to the polar direction of the BCTs and is, in fact, a domain wall separating two large-scale antiparallel domains (Supplementary Fig. 2). The formation of these two large domains can be explained by considering the mechanism of femtosecond laser poling. The nonlinear absorption of light results in a high temperature of the material in the laser focus (Fig. 2b). Consequently, the temperature gradient has two opposite projections on the *z* axis (which is also the direction of spontaneous polarization in the crystal) (Fig. 2c). Accordingly, the induced bipolar thermoelectric field (Fig. 2d) forces the originally random 180° domains to reorient in the direction of this electric field and to form two large antiparallel domains (Fig. 2e,f). Their visible elongated profile reflects the fact that for a cylindrically symmetric light intensity distribution in the focus, the *z* component of the induced thermoelectric field, responsible for poling, is asymmetric and drops faster in the direction normal to *z*, hence making domains narrower in that direction.

The QPM performance of the resultant 3D NPC was examined in terms of the simplest quadratic processes of second harmonic generation (SHG). Figure 3a presents an example of the harmonic intensity distribution obtained in simple tetragonal structures (with periods $\Lambda_x = 64.0\,\mu m$ and $\Lambda_y = \Lambda_z = 15.0\,\mu m$) at a fundamental wavelength of $\lambda_1 = 1.6\,\mu m$ (propagation along the *x* direction of the crystal). The emission consists of two types of pattern: (1) centrally located SH spots arranged into a square lattice and (2) peripheral spots situated relatively far from the direction of the pump beam and distributed along a set of homocentric rings (indexed as $h = -2$, -1, 0 in Fig. 3a).

Although the square lattice pattern is just a standard nonlinear Raman–Nath diffraction[24] (Supplementary Table 2), the appearance of peripheral SH spots is direct evidence of the 3D character of the nonlinear interaction. To show this we use the 3D QPM condition (Fig. 3b):

$$\mathbf{k}_2 = 2\mathbf{k}_1 + \mathbf{G}_{h,i,j} \qquad h, i, j \in \mathbb{Z}$$

where $\mathbf{k}_1, \mathbf{k}_2$ are wave vectors of the fundamental and SH beams, and $\mathbf{G}_{h,i,j} = h\mathbf{G}_a + i\mathbf{G}_b + j\mathbf{G}_c$ is a reciprocal lattice vector with $|\mathbf{G}_a| = 2\pi/\Lambda_X$, $|\mathbf{G}_b| = 2\pi/\Lambda_Y$ and $|\mathbf{G}_c| = 2\pi/\Lambda_Z$. Taking as an example
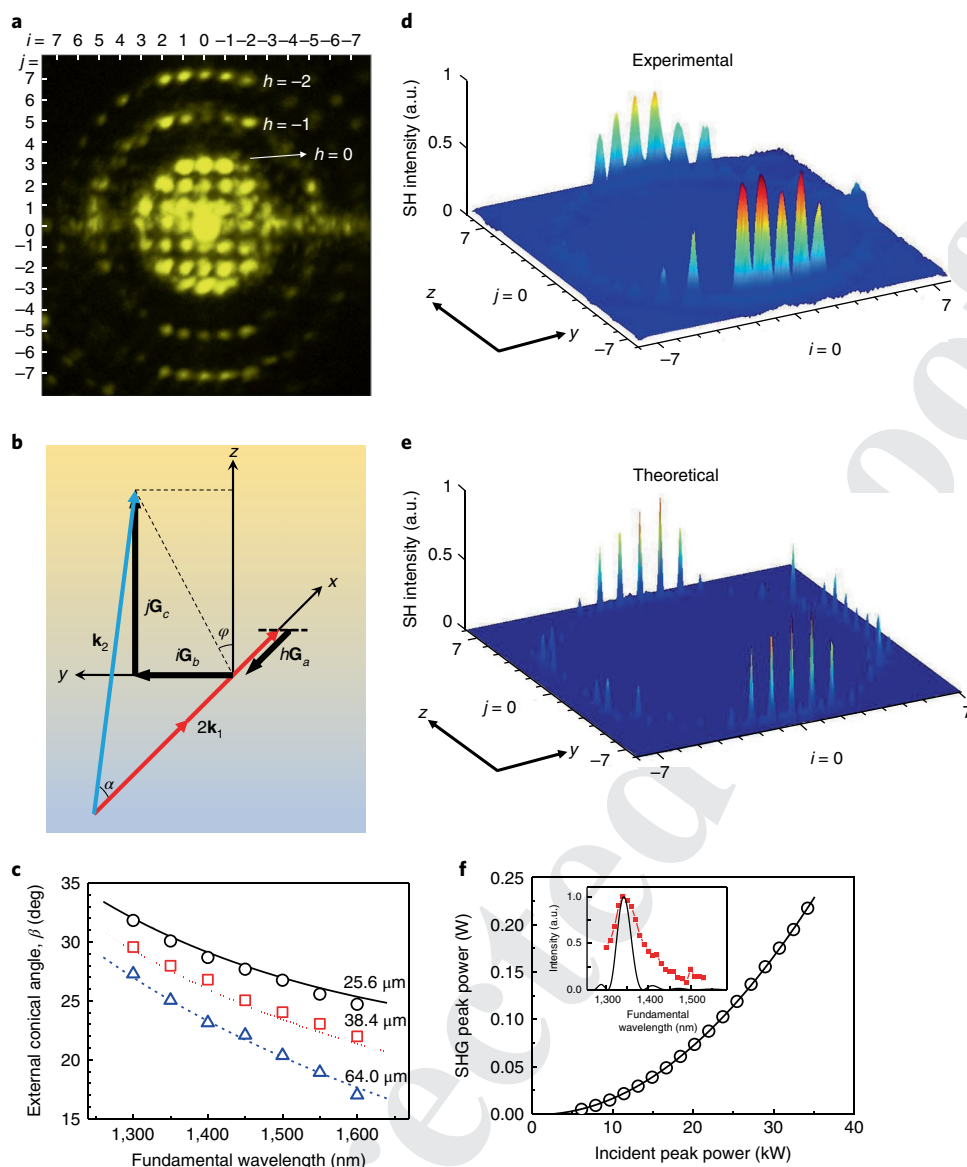
Fig. 3 | SHG in an all optically fabricated 3D NPC. a, Observed far-field SH pattern (at 800 nm) in a simple tetragonal ferroelectric domain structure (the colour is artificial for better visualization). **b**, 3D QPM diagram. **c**, Conical angle ($h = -1$) dependence on the fundamental wavelength for different longitudinal periods (Λ_x) of nonlinearity modulation. **d,e**, Experimental (**d**) and calculated (**e**) azimuthal intensity distribution of the SH spots corresponding to $h = -2$. **f**, Measured SHG power (dots) versus incident power from the domain pattern with $\Lambda_x = 25.6\,\mu m$. The fitting curve (line) shows a quadratic relationship. Inset, Resonance character of the interaction. The measured wavelength tuning response (dots) agrees well with the predicted response (line).

the generation of the strong spot SH$_{-2,1,7}$ ($h = -2$, $i = 1$, $j = 7$ in Fig. 3a), the phase matching in this process is mediated by the lattice vector $|\mathbf{G}|_{-2,1,7}$. To quantify the emission directions of various SH spots, two angles are required: the internal (external) conical angle α (β) between wavevector $\mathbf{k}_2$ and the x axis inside (outside) the crystal, and the azimuthal angle φ defined as the angle between the z axis and the projection of $\mathbf{k}_2$ onto the y–z plane (Fig. 3b). In the case of the SH$_{-2,1,7}$ signal, the measured external emission angles of $\beta = 22.98°$ and $\varphi = 8.04°$ agree well with the calculated values of $22.22°$ and $8.13°$. In a similar way, we can show that all observed SH bright spots originate from the interaction processes involving participation of certain 3D $\mathbf{G}_{h,i,j}$ vectors (Supplementary Table 1).

For a better understanding of the QPM 3D interaction we split the vectorial phase matching condition into longitudinal and transverse components:

$$k_2 \cos\alpha = 2k_1 + hG_a \qquad (1)$$

$$k_2 \sin\alpha = \sqrt{2(iG_b)^2 + (jG_c)^2} \qquad (2)$$

Fulfilment of longitudinal condition (1) is crucial to achieve an efficient SHG, as it ensures the monotonic power growth of SH with interaction distance. When this happens, the nonlinear interaction is also called nonlinear Čerenkov emission[25]. In a 2D interaction the Čerenkov emission is determined solely by the refractive indices of the fundamental and SH beams. This means that a single conical emission can normally be observed for a particular type of interaction. The situation is entirely different in a 3D NPC. In that case a series of conical Čerenkov-type SH beams are generated at angles α_h determined by the longitudinal periodic modulation of $\chi^{(2)}$

nonlinearity (Fig. 3c): $\alpha_h = \cos^{-1}[(n_1 + h\lambda_2 / \Lambda_X) / n_2]$, where n_1 and n_2 are the refractive indices of the nonlinear crystal at the fundamental and SH wavelengths, respectively. When the longitudinal modulation of nonlinearity is absent ($h = 0$), only the fundamental Čerenkov emission takes place at angle $\alpha_0 = \cos^{-1}(n_1/n_2)$.

The presence of transverse phase matching governed by equation (2) enhances the harmonic emission along specific transverse directions. When combined with Čerenkov emission, it defines the azimuthal position of the strong SH signals on the Čerenkov ring. It is precisely at these points where both transverse and longitudinal phase matching conditions are simultaneously satisfied, which represents fulfilment of the 3D nonlinear Bragg law. Hence, to obtain efficient emission of SHG at azimuthal angle φ, the transverse periods of the NPCs should be selected such that $\Lambda_Y = i\lambda_2 \sqrt{1 + \tan^2 \varphi} / (n_2 \sin \alpha)$ and $\Lambda_Z = j\Lambda_Y / (i \tan \varphi)$.

Notice that the SH intensity peaks on the Čerenkov rings are azimuthally nonuniform. They are generally stronger for an azimuthal angle close either to $\varphi = 0$ or π (Fig. 3d). In a regime of weak conversion, the intensity of a QPM SH is $I_2 \propto |\tilde{\chi}^{(2)}|^2 d_{eff}^2$, where $\tilde{\chi}^{(2)}$ denotes the Fourier transform of the nonlinearity modulation and d_{eff} is the effective nonlinearity that depends on both the polarization of the interacting beams and the emission direction within the crystal. Taking into account the specific θ shape of the individual inverted domains and the effective nonlinearity of our interaction geometry, we calculated the expected signal intensity (at $h = -2$) as a function of the azimuthal angle (Fig. 3e). This result agrees very well with experiments.

The conversion efficiency of SHG in the laser-induced 3D NPC was studied for collinear interactions (as an example). With a 128-μm-long domain pattern and longitudinal period of $\Lambda_x = 25.6\,\mu m$, we obtained a peak power of 2.3 W at $\lambda_2 = 670$ nm with 35 kW input (Fig. 3f). The normalized internal conversion efficiency, where the Fresnel reflections from the front and rear surfaces of the BCT crystal have been taken into account, is $1.7 \times 10^{-6}\,W^{-1}\,cm^{-1}$. The wavelength resonance of the collinear QPM SHG was also measured and agrees well with theory (Fig. 3f inset; see Supplementary Fig. 4 for more details). Notice that the resonance character of the interaction is clearly visible, even though our structure contains only a few longitudinal periods. This is a very encouraging result as it indicates that structures with extended longitudinal nonlinearity modulation should enable a frequency conversion that is sufficiently high for practical applications.

In conclusion, we have demonstrated a 3D NPC. This was created by 3D ferroelectric domain engineering with tightly focused femtosecond laser pulses in ferroelectric barium calcium titanate. The nonlinear absorption of light allows for the precise inversion of spontaneous polarization in the optical beam's focal volume inside transparent ferroelectrics. Although our work deals with a specific material, there seem to be no fundamental obstacles to the realization of similar structures in other types of ferroelectrics. Our first real example of 3D NPC is capable of compensating for the phase mismatch of second-order nonlinear optical processes along an arbitrary direction. As the optical poling method used here is fully compatible with other existing optical fabrication techniques, including the common femtosecond laser writing of refractive index structures, our results pave the way to achieving monolithic fabrication of 3D nonlinear integrated photonic devices for next-generation optical communications and on-chip signal processing.

Methods

Methods, including statements of data availability and any associated accession codes and references, are available at https://doi.org/10.1038/s41566-018-0225-1.

References

1. Armstrong, J. A., Bloembergen, N., Ducuing, J. & Pershan, P. S. Interactions between light waves in a nonlinear dielectric. *Phys. Rev.* **127**, 1918–1939 (1962).
2. Berger, V. Nonlinear photonic crystals. *Phys. Rev. Lett.* **81**, 4136–4139 (1998).
3. Broderick, N. G. R., Ross, G. W., Offerhaus, H. L., Richardson, D. J. & Hanna, D. C. Hexagonally poled lithium niobate: a two-dimensional nonlinear photonic crystal. *Phys. Rev. Lett.* **84**, 4345–4348 (2000).
4. Arie, A. & Voloch, N. Periodic, quasi-periodic, and random quadratic nonlinear photonic crystals. *Laser Photon. Rev.* **4**, 355–373 (2010).
5. Ellenbogen, T., Voloch-Bloch, N., Ganany-Padowicz, A. & Arie, A. Nonlinear generation and manipulation of Airy beams. *Nat. Photon.* **3**, 395–398 (2009).
6. Canalias, C. & Pasiskevicius, V. Mirrorless optical parametric oscillator. *Nat. Photon.* **1**, 459–462 (2007).
7. Zhang, Y., Wen, J., Zhu, S. N. & Xiao, M. Nonlinear Talbot effect. *Phys. Rev. Lett.* **104**, 183901 (2010).
8. Greve, K. et al. Quantum-dot spin-photon entanglement via frequency down-conversion to telecom wavelength. *Nature* **491**, 421–425 (2012).
9. Leng, H. Y. et al. On-chip steering of entangled photons in nonlinear photonic crystals. *Nat. Commun.* **2**, 429 (2011).
10. Zhu, S. N., Zhu, Y. Y. & Ming, N. B. Quasi-phase-matched third-harmonic generation in a quasi-periodic optical superlattice. *Science* **278**, 843–846 (1997).
11. Chen, J. J. & Chen, X. F. Phase matching in three-dimensional nonlinear photonic crystals. *Phys. Rev. A* **80**, 013801 (2009).
12. Pogosian, T. & Lai, N. D. Theoretical investigation of three-dimensional quasi-phase-matching photonic structures. *Phys. Rev. A* **94**, 063821 (2016).
13. Bahabad, A. & Arie, A. Generation of optical vortex beams by nonlinear wave mixing. *Opt. Express* **15**, 17619–17624 (2007).
14. Guo, R. et al. Non-volatile memory based on the ferroelectric photovoltaic effect. *Nat. Commun.* **4**, 1990 (2013).
15. Shur, V. Ya et al. Domain kinetics in the formation of a periodic domain structure in lithium niobate. *Phys. Solid State* **41**, 1681–1687 (1999).
16. Ying, C. Y. J. et al. Light-mediated ferroelectric domain engineering and micro-structuring of lithium niobate crystals. *Laser Photon. Rev.* **6**, 526–548 (2012).
17. Steigerwald, H. et al. Direct writing of ferroelectric domains on the x- and y-faces of lithium niobate using a continuous wave ultraviolet laser. *Appl. Phys. Lett.* **98**, 062902 (2011).
18. Boes, A. et al. Direct writing of ferroelectric domains on strontium barium niobate crystals using focused ultraviolet laser light. *Appl. Phys. Lett.* **103**, 142904 (2013).
19. Segal, N., Keren-Zur, S., Hendler, N. & Ellenbogen, T. Controlling light with metamaterial-based nonlinear photonic crystals. *Nat. Photon.* **9**, 180–184 (2015).
20. Li, G. X., Zhang, S. & Zentgraf, T. Nonlinear photonic metasurfaces. *Nat. Rev. Mater.* **2**, 17010 (2017).
21. Chen, X. et al. Ferroelectric domain engineering by focused infrared femtosecond pulses. *Appl. Phys. Lett.* **107**, 141102 (2015).
22. Chen, X. et al. Quasi-phase matching via femtosecond laser-induced domain inversion in lithium niobate waveguides. *Opt. Lett.* **41**, 2410–2413 (2016).
23. Chen, X. et al. Ferroelectric domain patterning with ultrafast light. *Opt. Photon. News* **27**, 50 (2016).
24. Saltiel, S. M. et al. Generation of second-harmonic conical waves in nonlinear Bragg diffraction. *Phys. Rev. Lett.* **100**, 103902 (2008).
25. Saltiel, S. M. et al. Cerenkov-type second-harmonic generation in two-dimensional nonlinear photonic structures. *IEEE J. Quantum Electron.* **45**, 1465–1472 (2009).

Author contributions

Y.S. and W.K. conceived and coordinated the research project. All authors made significant contributions to the experiments, analysis of the data and writing of the manuscript.

Competing interests

The authors declare no competing interests.

Additional information

Supplementary information is available for this paper at https://doi.org/10.1038/s41566-018-0225-1.

Reprints and permissions information is available at www.nature.com/reprints.

Correspondence and requests for materials should be addressed to Y.S. or W.K.

Publisher's note: Springer Nature remains neutral with regard to jurisdictional claims in published maps and institutional affiliations.

Methods

Direct laser writing of 3D ferroelectric domain patterns. We used a 500-µm-thick X-cut BCT wafer. The sample was mounted on a translational stage that could be positioned in three orthogonal directions with a resolution of 100 nm. The infrared writing optical beam originated from a femtosecond oscillator (MIRA, Coherent) operating at 815 nm, with a pulse duration of 180 fs and repetition rate of 76 MHz. The optical beam, polarized along the y direction of the crystal, was incident normally at the BCT, and was focused by a ×20 microscope objective (NA = 0.4) into the sample. The beam diameter in focus was estimated to be ~2 µm. The energy of the incoming pulses could be continuously varied using a half-wave plate followed by a polarizer, and a typical value of ~6 nJ was used in the experiments. The domain inversion process involved illuminating the crystal for 0.5 s. The shutter then blocked the beam and the sample was moved to another location where the process was repeated. In the experiment we found that 3D domain inversion in the BCT crystal can occur within a range of pulse energies above a certain minimum value and below the damage threshold of the material. The writing threshold was about 3.1 nJ at a depth of 50 µm below the crystal surface. High-energy pulses and a longer exposure time were found to be beneficial for increasing the size of the inverted domains. Because the femtosecond laser writing is based on two-photon absorption, there is a requirement for the wavelength to be short enough to excite the two-photon process.

The domain structures were typically fabricated at a depth of 50–350 µm below the surface of the crystal. The achievable number of domain periods along the depth of the crystal is mainly restricted by the focusing condition of the femtosecond laser beam, which worsens with depth due to aberrations. This is a common issue in femtosecond laser writing, especially for materials with high refractive indices and when writing deep inside a medium. However, these adverse effects can be minimized by taking special measures, such as pre-shaping the beam using a spatial light modulator and selecting the polarization to avoid focus splitting[26] so that much longer samples can be fabricated. Operating in the transverse plane (y–z in our case) is relatively hassle-free, and large-area structures can be easily formed. In our case of a BCT crystal, 3D domain structures are created inside the 180° domain regions, which are sandwiched between neighbouring 90° domain walls, so the size of the former regions restricts the area of laser domain reversal.

Characterization of the laser-inscribed ferroelectric domain patterns. Fabricated domain patterns were visualized by Čerenkov SH microscopy[27]. This is based on strong Čerenkov SHG from the boundaries of steep $\chi^{(2)}$ variation. Therefore, the bright areas in the Čerenkov microscopy images correspond to ferroelectric domain walls. Consequently, the central horizontal line in the θ-shaped structure separates two oppositely oriented large domains. Čerenkov SHG microscopy was carried out using a commercial Zeiss LSM 780 scanning confocal microscope, coupled with a femtosecond laser source (Mai Tai Spectra Physics) operating at 900 nm.

We also checked that annealing the sample at high temperature above the Curie point of 108 °C leads to erasure of the domains, leaving a homogeneous area of the crystal that could then be rewritten with a new domain pattern (Supplementary Fig. 5).

It is well known that localized ferroelectric domains are often accompanied by a refractive index change in the vicinity of domain walls[28], which leads to linear diffraction of light[29]. However, in our experiments we did not observe any clear linear diffraction, nor any additional propagation loss of the fundamental beam caused by the inscribed periodic domain patterns. This confirms that the potential linear refractive index modulation did not contribute to the nonlinear interaction observed in our experiments.

SHG experiment with 3D domain structures. The fundamental beam was provided by a femtosecond optical parametric oscillator (Chameleon, Coherent). The wavelength could be tuned between 1 µm and 1.60 µm, with a pulse duration of 150 fs and repetition rate of 80 MHz. The beam propagated along the x axis of the crystal and was polarized along the y direction to make use of the largest nonlinear coefficient d_{32} in the frequency conversion process. The beam was loosely focused at the domain structure using a ×4 objective lens (NA = 0.1) to produce a spot of about 50 µm in diameter. A short-pass filter was used to block the fundamental beam. The emitted SH signal was projected to a screen in the far field, and the image was recorded using a charge-coupled device camera. The SH ring on the screen should, in general, be slightly elliptical, because BCT is a birefringent crystal. However, because this birefringence is rather weak (n_o = 2.3558, n_e = 2.3156 at 800 nm), calculations show deviation from a circle of ~0.34° for the fundamental Čerenkov ring (h = 0 in Fig. 3a), which is negligible. It should also be noted that the naturally random domains of BCT crystals lead to a background SH emission[30]. However, this effect was so weak compared to the signals originating from the 3D structure that it could be neglected (Supplementary Fig. 1).

Data availability. The data that support the results within this paper and other findings of the study are available from the corresponding authors upon reasonable request.

References

26. Karpinski, P., Shvedov, V., Krolikowski, W. & Hnatovsky, C. Laser-writing inside uniaxially birefringent crystals: fine morphology of ultrashort pulse-induced changes in lithium niobate. *Opt. Express* **24**, 7456–7476 (2016).
27. Sheng, Y. et al. Three-dimensional ferroelectric domain visualization by Čerenkov-type second harmonic generation. *Opt. Express* **18**, 16539–16545 (2010).
28. Kim, S. & Gopalan, V. Optical index profile at an antiparallel ferroelectric domain wall in lithium niobate. *Mater. Sci. Eng. B* **120**, 91–94 (2005).
29. Müller, M. et al. Investigation of periodically poled lithium niobate crystals by light diffraction. *J. Appl. Phys.* **97**, 044102 (2005).
30. Xu, T. X. et al. A naturally grown three-dimensional nonlinear photonic crystal. *Appl. Phys. Lett.* **108**, 051907 (2016).

QUERY FORM

Nature Photonics	
Manuscript ID	**[Art. Id: 225]**
Author	**Tianxiang Xu**

AUTHOR:

The following queries have arisen during the editing of your manuscript. Please answer by making the requisite corrections directly in the e.proofing tool rather than marking them up on the PDF. This will ensure that your corrections are incorporated accurately and that your paper is published as quickly as possible.

Query No.	*Nature of Query*
Q1:	Please check that the abstract is OK as amended.
Q2:	Please check that the first paragraph of the main text is OK as amended.
Q3:	Author surnames have been highlighted - please check these carefully and indicate if the first name or surname have been marked up incorrectly. Please note that this will affect indexing of your article, such as in PubMed.
Q4:	Please note that the eproof should be amended in only one browser window at any one time, otherwise changes will be overwritten.
Q5:	Please check that the sentence beginning "Motivated" is OK as amended.
Q6:	Please clarify what you mean by X-cut here.
Q7:	Please check that the caption to Figure 2 is OK as amended.
Q8:	Please check that the sentence beginning "The QPM performance" is OK as amended.
Q9:	Please note that journal style uses bold upright font for vectors. Please check throughout that this has been applied correctly.
Q10:	There is no ref 37 in this paper, but ref 29 was not cited and seems relevant here, so I have changed 37 to 29 - please check this and amend if this is not correct.
Q11:	Please check that the sentence beginning "However" is OK as amended.